Available online at www.sciencedirect.com
SCIENCE DIRECT®
ELSEVIER
Journal of Computational and Applied Mathematics 193 (2006) 219–242
JOURNAL OF COMPUTATIONAL AND APPLIED MATHEMATICS
www.elsevier.com/locate/cam

A pseudospectral method of solution of Fisher's equation

Daniel Olmos, Bernie D. Shizgal*,[1]

Institute of Applied Mathematics, University of British Columbia, Vancouver, British Columbia, Canada V6T 1Z1

Received 6 January 2005

Abstract

In this paper, we develop an accurate and efficient pseudospectral solution of Fisher's equation, a prototypical reaction–diffusion equation. The solutions of Fisher's equation are characterized by propagating fronts that can be very steep for large values of the reaction rate coefficient. There is an ongoing effort to better adapt pseudospectral methods to the solution of differential equations with solutions that resemble shock waves or fronts typical of hyperbolic partial differential equations. The collocation method employed is based on Chebyshev–Gauss–Lobatto quadrature points. We compare results for a single domain as well as for a subdivision of the main domain into subintervals. Instabilities that occur in the numerical solution for a single domain, analogous to those found by others, are attributed to round-off errors arising from numerical features of the discrete second derivative matrix operator. However, accurate stable solutions of Fisher's equation are obtained with a multidomain pseudospectral method. A detailed comparison of the present approach with the use of the sinc interpolation is also carried out.

Keywords: Fisher equation; Pseudospectral method; Sinc interpolation; Round-off error

1. Introduction

Spectral methods have long been known to provide very accurate and rapidly convergent solutions of partial differential equations with smooth solutions [9,12,40]. These methods generally provide an exponential convergence of the solution versus the number of collocation points. In recent years, spectral

* Corresponding author.
E-mail address: shizgal@chem.ubc.ca (B.D. Shizgal).
[1] Also with the Department of Chemistry, University of British Columbia, 2036 Main Mall, Vancouver, British Columbia, Canada V6T 1Z1.

0377-0427/$ - see front matter © 2005 Elsevier B.V. All rights reserved.
doi:10.1016/j.cam.2005.06.028

methods have also been used for the solution of differential equations with solutions that resemble shock waves or fronts typical of hyperbolic partial differential equations [22]. There is an ongoing interest to further adapt spectral methods to differential equations with rapidly varying and propagating solutions.

The purpose of the present paper is to apply a spectral method to the solution of Fisher's equation (FE), which was original proposed by Fisher [19] as a model for the spatial and temporal propagation of a virile gene in an infinite medium. It is a one-dimensional reaction diffusion model for the evolution of the infected population, $U(x', t')$, with a quadratic reactive term corresponding to logistic growth. The equation is defined by

$$\frac{\partial U}{\partial t'} = D\frac{\partial^2 U}{\partial x'^2} + kU(1-U), \tag{1}$$

where t' is the time and $x' \in (-\infty, \infty)$ is the position. The diffusion and reactive processes are parameterized by a diffusion coefficient, D, and a reactive rate coefficient, k, respectively. We consider solutions to Eq. (1) subject to the following initial and boundary conditions,

$$\begin{aligned} &\lim_{x'\to\infty} U(x', t') = 0, \\ &\lim_{x'\to-\infty} U(x', t') = 1, \\ &U(x', 0) = U_0(x'). \end{aligned} \tag{2}$$

It has been shown that with the appropriate boundary conditions FE will support travelling waves of the form $U(x' - c't')$ moving in the positive x-direction, provided that the speed c' is greater than the critical value $c'_{\min} = 2\sqrt{kD}$. Eq. (1) is the simplest reaction–diffusion equation employed to model many problems in mathematical biology [36]. With the change of variables,

$$t = kt', \quad x = x'\left(\frac{k}{D}\right)^{1/2}$$

Eq. (1) becomes

$$\frac{\partial U}{\partial t} = \frac{\partial^2 U}{\partial x^2} + U(1-U) \tag{3}$$

and travelling wave solutions exist for dimensionless speeds $c \geqslant 2$, [28].

The mathematical properties of FE have been studied extensively and there have been numerous discussions in the literature. Excellent summaries have been provided in [10,29,36]. One of the first numerical solutions was presented in [21] with a pseudo-spectral approach. Implicit and explicit finite differences algorithms, have been reported by different authors such as Parekh and Puri [39] and Twizell et al. [49]. The works of Mickens [33,34] considered time stepping aspects for finite difference algorithms. The work in [25], where the main goal was to develop asymptotic boundary conditions, considered a centered finite difference algorithm. Rizwan-Uddin [43] compared a nodal method with nonstandard finite differences scheme. A Galerkin finite element method was used by Tang and Weber [48] whereas Carey and Shen [13] employed a least-squares finite element method. A collocation approach based on Whittaker's sinc interpolation function [9,47] was also considered in [2,58]. The work in [23] considered a nonlocal form of FE. The study in [59] was concerned with another modified form of FE including time delay and the work in [44] considered finite elements for a two-dimensional FE.

Solutions of FE exhibiting propagating fronts thus possess features similar to those of shock waves that arise with hyperbolic equations. There are also special interesting features of the solution in terms of the relation between the speed of the wavefront and the behavior of the solution at infinity [24,29]. Larson [29] and Hagan [24] proved that for any initial condition of Eq. (3) such that

$$U_0(x) \quad \overrightarrow{x \to \infty} \quad A\mathrm{e}^{-\beta x}$$

then, $U(x,t)$ evolves as a wave front with speed given by

$$c = \begin{cases} \beta + \frac{1}{\beta} & 0 < \beta \leqslant 1, \\ 2 & \beta \geqslant 1. \end{cases}$$

There is also an interest concerning the instability of the solution to small perturbations in the solution particularly when $U(x,t) \approx 0$ as discussed by different authors [11,21,24,41]. Canosa [11] proved stability of the solution to perturbations of compact support, whereas instability occurred when the perturbation vanished at infinity. This property plays a fundamental role when Eq. (3) is solved numerically [21].

A closely related problem is to consider a modified form of FE introduced in [30], for which the nonlinear reactive term is made arbitrarily larger than the diffusion term. This modified FE is given by

$$\frac{\partial U}{\partial t} = \frac{\partial^2 U}{\partial x^2} + \rho U(1-U) \tag{4}$$

with initial and boundary conditions similar to Eq. (2), and the reaction rate coefficient is generally chosen so that $\rho \gg 1$. A particular solution of Eq. (4) considered in [30], was found by Ablowitz and Zepetella [1]. It has the form of a travelling wave front, and is given by

$$U(x,t) = \frac{1}{(1+\exp^{\sqrt{\rho/6}x - 5\rho/6t})^2} \tag{5}$$

which travels with constant speed $c = 5\sqrt{\rho/6}$. The initial condition of Eq. (4) is clearly given by $U_0(x) = U(x,0)$. Solutions of Eq. (4) with large ρ have been referred in [58] as super speed wave (SSW) types. With an increase in ρ, the propagating front steepens and this presents a challenging numerical problem to both resolve and track the front. This rescaled version of FE was considered by Li et al. [30] in their study of moving mesh strategies in finite difference methods of solution of partial differential equations. They commented that moving mesh methods are not recommended for such reaction diffusion problems for which the diffusion term is much smaller than the reactive term. Subsequently, Qiu and Sloan [41] carried out a detailed comparison of different moving mesh strategies [26,27] and concluded that these methods are not easily adapted for equations analogous to FE with steep fronts. The authors have also applied these methods to Burger's equation [7,8,35] with similar shock like solutions. In the course of these studies on FE, numerous workers have also reported a sensitivity of the numerical solutions to perturbations owing to numerical noise in the solutions or round-off errors resulting in instabilities.

One of the objectives of the present paper is to apply spectral methods to the solution of FE. A second objective is to establish a relationship between the problems given by Eqs. (3) and (4), which we demonstrate lead to equivalent numerical problems. In the first instance, we consider a single fixed domain suitably truncated to the interval $[x_L, x_R]$ and apply a spectral method based on Chebyshev–Lobatto points. This approach gives good results but only for relatively small values of ρ. The difficulty encountered for

larger values of ρ is traced to round-off errors in the application of the second derivative spectral matrix operator to the solution. The occurrence of round-off errors for these matrix derivative operators have been well documented [3–5]. We examine in detail the origin of these round-off errors in the application of spectral methods to FE. A multidomain approach developed in [31,56,57] for the solution of Burgers equation and the Navier Stokes equation was then employed for the present work. We obtain accurate stable solutions of FE for relatively large values of ρ, with the appropriate division of the domain $[x_L, x_R]$ into subdomains. In Section 2, we outline our spectral method applied to FE in one domain and analyze the problem of round-off errors. The multidomain approach is presented in Section 3. In Section 4, we present a comparison of the present approach with the one based on Whittaker's sinc interpolation [9,16,55] employed in [58,50] that they refer to as the discrete singular convolution (DSC).

2. Chebyshev–Lobatto spectral approach to Fisher's equation

2.1. The modified FE; scaling the ρ dependence

Several groups [30,41,58], have employed the modified form of FE (Eq. (4)) for the SSW situation. The exact solution of the modified FE exhibits a shock-like front for large ρ and speed $c = 5\sqrt{\rho/6}$. For the infinite spatial domain, the rapidly varying shock front is considered to be stiff with the stiffness depending on ρ. In the next section, we propose a numerical solution of Eq. (4) which involves the expansion of the solution in Chebyshev polynomials orthogonal on $[-1, 1]$. This requires that the boundary conditions be applied on a truncated domain $[x_L, x_R]$. As a consequence of the use of a finite domain in the numerical solution, there is an important dependence of the solution on ρ and the width of the interval considered. On this truncated interval, we consider the differential equation for $V(x, t)$,

$$V_t = V_{xx} + \rho V(1 - V) \tag{6}$$

with the initial condition given by

$$V(x, 0) = V_0(x), \quad x \in [x_L, x_R] \tag{7}$$

and boundary conditions at the ends of the truncated interval, that is

$$\begin{aligned} &V(x_L, t) = 1, \\ &V(x_R, t) = 0, \quad t \in [0, T] \end{aligned} \tag{8}$$

where $V_0(x)$ is given by $U(x, 0)$ in Eq. (5) but over $[x_L, x_R]$. From Eq. (5), the dependence on the parameter ρ can be removed with a scaling of the space and time variables, i.e.

$$z = \sqrt{\rho}x, \quad \tau = \rho t \tag{9}$$

and Eq. (6) can be written with the dependence of ρ occurring only at the end points of the computational domain, that is

$$V_\tau = V_{zz} + V(1 - V) \tag{10}$$

with

$$\begin{aligned} &V(z,0) = V_0(z), \quad z \in [\sqrt{\rho}x_{\mathrm{L}}, \sqrt{\rho}x_{\mathrm{R}}] \\ &V(\sqrt{\rho}x_{\mathrm{L}}, \tau) = 1, \\ &V(\sqrt{\rho}x_{\mathrm{R}}, \tau) = 0, \quad \tau \in [0, \rho T]. \end{aligned} \tag{11}$$

Due to the boundary condition $V\left(\sqrt{\rho}x_{\mathrm{R}}, \tau\right) = 0$, and in order to preserve a good approximation of the solution. T is taken as a time before the wavefront hits the right boundary at x_{R}.

By virtue of the transformations Eq. (9), the solution of Eq. (6) for $\rho = \rho_1$ on $[x_{\mathrm{L}}, x_{\mathrm{R}}]$ is equivalent to Eq. (10) on $[\sqrt{\rho_1}x_{\mathrm{L}}, \sqrt{\rho_1}x_{\mathrm{R}}]$. Similarly, the solution for $\rho = \rho_2$ on $[x'_{\mathrm{L}}, x'_{\mathrm{R}}]$ is equivalent to Eq. (10) on $[\sqrt{\rho_1}x'_{\mathrm{L}}, \sqrt{\rho_1}x'_{\mathrm{R}}]$. The solutions for different ρ are equivalent to each other provided that

$$x'_{\mathrm{L}} = \sqrt{\frac{\rho_1}{\rho_2}}\, x_{\mathrm{L}}, \quad x'_{\mathrm{R}} = \sqrt{\frac{\rho_1}{\rho_2}}\, x_{\mathrm{R}} \tag{12}$$

are satisfied. If we consider the problem given by Eq. (6) with $\rho = \rho_2$ on $[x'_{\mathrm{L}}, x'_{\mathrm{R}}]$, and a numerically equivalent problem given by ρ_1 on $[x_{\mathrm{L}}, x_{\mathrm{R}}]$ (i.e. satisfying (12)), then, if ρ_1 is modified to $\overline{\rho}_1$, the problem with $\rho = \rho_2$ on $[x'_{\mathrm{L}}, x'_{\mathrm{R}}]$ and the modified problem with $\rho = \overline{\rho}_1$ on $[x_{\mathrm{L}}, x_{\mathrm{R}}]$, are no longer equivalent unless x_{L} and x_{R} are modified in order to satisfy condition (12). In other words, relation (12) establishes a property between ρ and the length of the interval $L = x_{\mathrm{R}} - x_{\mathrm{L}}$, where modifying ρ or L and fixing the other one, represents the same problem as long as relation (12) is satisfied. It follows that increasing the value of ρ leads to a steeper front only if we consider a fixed numerical domain. This aspect of FE appears not to have been mentioned previously in the literature.

The case of SSW studied in [30,41,58] has been considered previously by different authors with $\rho = 1$ and different interval lengths. As an example, Qiu and Sloan [41] and Zhao and Wei [58] considered the computational domain with end points given by $x_{\mathrm{L}} = -0.2$ and $x_{\mathrm{R}} = 0.8$ with $\rho = 10^4$ whereas Gazdag and Canosa [21] considered $\rho = 1$, $x_{\mathrm{L}} = 0$, $x_{\mathrm{R}} = 140$. According to (9), the problem considered in [21], is equivalent to $\rho = (140)^2 = 19,600$, $x_{\mathrm{L}} = 0$ and $x_{\mathrm{R}} = 1$. Another example is the problem studied in [39] where they chose $\rho = 1$, $x_{\mathrm{L}} = 0$ and $x_{\mathrm{R}} = 300$ which is equivalent to $\rho = (300)^2 = 90,000$ with $x_{\mathrm{L}} = 0$ and $x_{\mathrm{R}} = 1$. However, these previous works did not consider the case of solving Eq. (6), with the initial and boundary conditions given by Eqs. (7) and (8). Instead, properties such as the numerical stability of algorithms, or features of reaction diffusion processes, were considered. As an example of previous numerical studies, we mention the works in [2,13,43,48] that analyzed the phenomena of reaction and diffusion on FE for different initial conditions. Gazdag and Canosa [21] based on Canosa's previous work [11], considered initial conditions of Eq. (3) with an asymptotic behavior at infinity such that the speed is faster than the minimum, $c = 2$. However, due to their proposed numerical scheme, they obtained oscillations in their numerical solution near the right boundary and at the onset of the front, giving an unstable solution. The instability problem was solved considering $V(x,t) = 0$ whenever $|V(x,t)| < \varepsilon$, where ε is some small quantity. However, this assumption leads to the loss of the initial theoretical speed, and to the convergence to the minimum speed front $c = 2$.

The variable ρ in the numerical problem (10) with (11), does not play the role of a reaction rate coefficient but a scaling over the numerical domain as considered in [2,13,21,39,43,48]. However, as the work presented in this paper follows from the work by Li et al. [30] and [41,58], we will consider the numerical problem given by (6) with (7).

2.2. Pseudospectral solution of the modified FE

We expand $U(x,t)$ or $V(x,t)$ in the Chebyshev polynomials, $T_k(x)$, which are orthogonal with respect the weight function $w(x) = (1-x^2)^{-1/2}$ on the interval $[-1, 1]$, that is,

$$\frac{1}{c_k}\int_{-1}^{1} w(x)T_k(x)T_l(x)\,\mathrm{d}x = \frac{1}{2}\pi\delta_{k,l}, \tag{13}$$

where $c_k = 1$ for all k except for $c_0 = 2$. The Lobatto quadrature points and weights associated with the Chebyshev polynomials are given by $x_i = -\cos(\pi i/N)$ and the weights are $w_i = \pi/N$ for all i except $w_0 = w_N = \pi/2N$ [9,12,40]. These points and weights provide the approximate quadrature,

$$\int_{-1}^{1} w(x)f(x)\,\mathrm{d}x \simeq \sum_{i=0}^{N} w_i f(x_i), \tag{14}$$

where $N+1$ is the number of points. Since any piecewise continuous function, $f \in L_w^2[0,1]$ can be expanded in a Chebyshev polynomial series that is convergent in the L_w^2 norm, we have

$$f(x) \approx f_N(x) = \sum_{k=0}^{N} a_k T_k(x), \tag{15}$$

where

$$a_k = \frac{2}{c_k\pi}\int_{-1}^{1} w(x)f(x)T_k(x)\,\mathrm{d}x. \tag{16}$$

With Eqs. (14)–(16) we obtain the interpolation algorithm

$$f_N(x) \simeq \sum_{j=0}^{N} I_j(x)f(x_j), \tag{17}$$

where the interpolating polynomials, $I_j(x)$, are given by

$$I_j(x) = \frac{2}{Nv_j}\sum_{k=0}^{N} v_k T_k(x_j)T_k(x), \tag{18}$$

where $v_0 = v_N = 1/2$ and $v_k = 1$ if $k \neq 0, N$. The nth derivative of $f(x)$ at the quadrature points is then given approximately by

$$f_N^{(n)}(x_k) \simeq \sum_{j=0}^{N} I_j^{(n)}(x_k)f(x_j). \tag{19}$$

If we denote by $\mathbf{f}$, the vector of the function evaluated at the Chebyshev–Lobatto points, Eq. (19) can be rewritten as

$$\mathbf{f^{(n)}} = \mathbf{D^{(n)}}\cdot\mathbf{f} \tag{20}$$

and thus, the second derivative matrix is then identified with

$$D^{(2)}_{jk} = \left.\frac{d^2 I_j(x)}{\mathrm{d}x^2}\right|_{x=x_k} \tag{21}$$

This is the basis for the Chebyshev pseudospectral method.

It is now straightforward to apply the pseudospectral method to the modified FE, by approximating the second derivative operator as in Eq. (21). From Eq. (6) and the linear transformation from $[x_\mathrm{L}, x_\mathrm{R}]$ to $[-1, 1]$, the following system of ordinary differential equations is obtained.

$$\frac{\mathrm{d}V_i}{\mathrm{d}t} = A\sum_{j=0}^{N} D^{(2)}_{ij} V_j + \rho V_i(1 - V_i), \tag{22}$$

where $A = 4/(x_\mathrm{R} - x_\mathrm{L})^2$, $V_i = V(x_i, t)$ and the time dependence is considered implicitly in V_i. The spectral derivative matrices were calculated with the MATLAB suite of programs developed in [54]. The set of ordinary differential equations was integrated with a Runge–Kutta integrator in MATLAB subject to the boundary conditions, $V(x_\mathrm{L}) = 1$ and $V(x_\mathrm{R}) = 0$ for all t.

2.3. Numerical results

The formalism in Sections 2.1 and 2.2 was applied to a study of the behavior of the numerical solution of FE versus ρ. The behavior for a fixed interval for different values of ρ is considered. In the present study, $U_0(x)$ will refer to the initial condition depending on ρ, that is Eq. (5) with $t = 0$, unless it is otherwise indicated. We choose $x_\mathrm{L} = -0.2$, $x_\mathrm{R} = 0.8$ as done in [41,58] and vary ρ. In Fig. 1, we compare the analytic solution $U(x, t)$ (solid curves) evaluated at the Chebyshev collocation points with the numerical solution V_i (symbols), at different t. The values of ρ are (A) 2000, (B) 5000 and (C,D) 10,000, and we note that $\rho = 10,000$ was considered in the previous works [30,41,58]. The steepening of the front on increasing ρ for a fixed interval is clearly seen by comparing Figs. 1C and D with Figs. 1A and B. In Fig. 1A, the good agreement between the numerical results and the analytic solution with $\rho = 2000$ and 40 Chebyshev points is shown. As the initial profile (Eq. (5), $t = 0$) behaves asymptotically as given by Eq. (28), the wave speed is constant at $c = 5\sqrt{\rho/6}$. The wave speeds calculated from the numerical solutions agree with the theoretical speed to 4–6 significant figures depending on the value of ρ. In order to get a stable and accurate solution for $\rho = 5000$ shown in Fig. 1B, the number of points had to be increased from $N = 40$ to 64. Fig. 1C for $\rho = 10^4$ and $N = 64$, shows an instability (negative part) that appears at $x \sim 0.7$ for $t = 0.002$. When N is increased to 150, a stable solution is obtained as shown in Fig. 1D. To further validate the numerical method used, we have considered the solution of the diffusion equation ($\rho = 0$) but with an exponentially decaying initial profile ($U_0(x)$, $\rho = 10^4$). We find that instabilities at small times are quickly damped by diffusion. However, for FE with $\rho = 1.5 \times 10^4$, a stable solution could not be obtained even with N as large as 250.

It is of considerable interest to understand the origin of this instability, which we attribute to round-off error associated with the application of the second derivative operator on the solution at some time step. This is a problem common to many applications of spectral methods as recently discussed [3–5]. We therefore study the error in the numerical computation of the second derivative of the initial condition

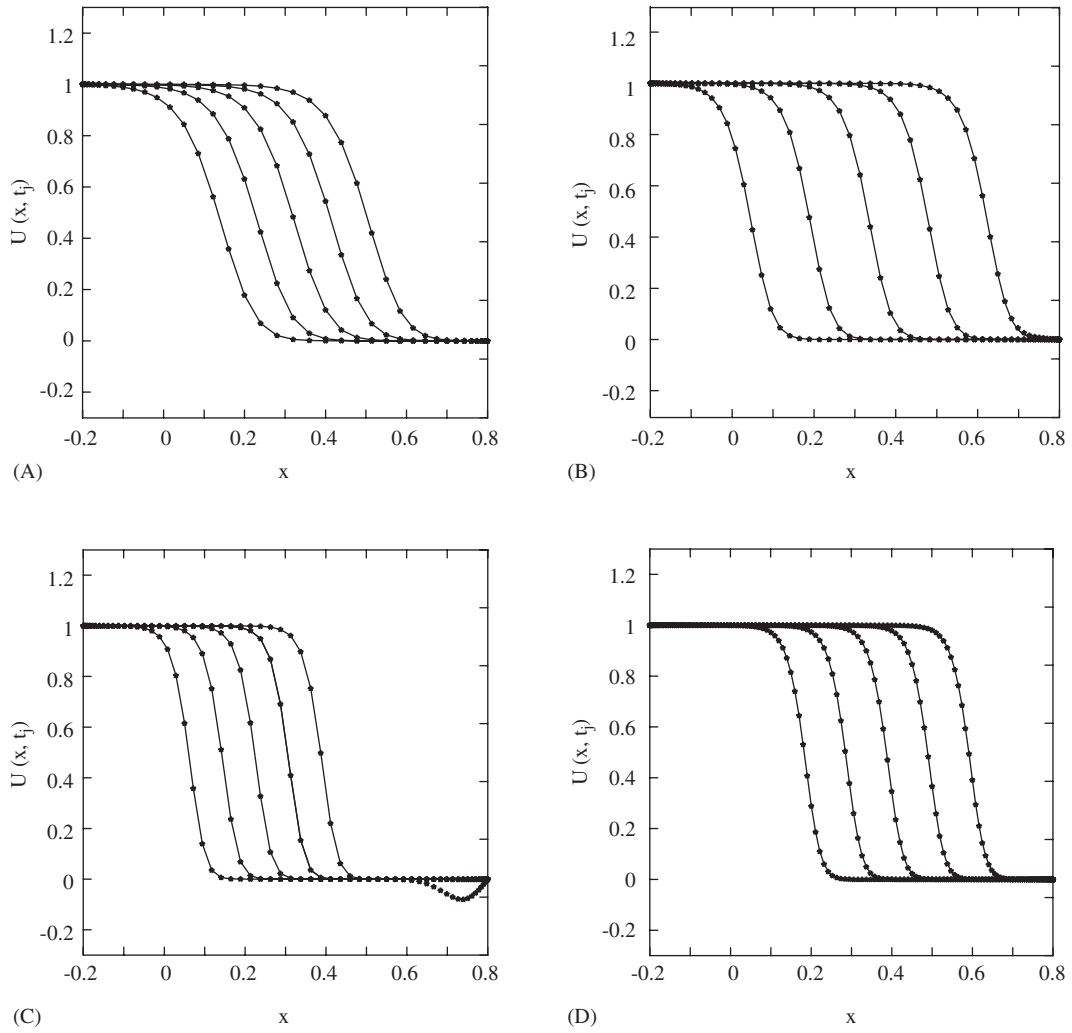

Fig. 1. Time dependent profiles versus x for ρ and N equal to (A) 2×10^3, 40; (B) 5×10^3, 64; (C) 10^4, 64 and (D) 10^4, 150. The successive profiles in each graph are for times (A) $t = 0.002, 0.003, 0.004, 0.005, 0.006$; (B) $t = 0.0005, 0.0015, 0.0025, 0.0035, 0.0045$; (C) $t = 0.0004, 0.0008, 0.0012, 0.0016, 0.002$; (D) $t = 0.001, 0.0015, 0.002, 0.0025, 0.003$. The solid line represents the analytic solution, $U(x, t)$, and the symbols, V_i, the numerical solution evaluated at the Chebyshev points.

$U_0(x)$. In Fig. 2, we show the relative error defined by

$$R_{\mathrm{E}}(x_k) = \log_{10} \left| \frac{\partial^2 U_0(x)/\partial x^2|_{x=x_k} - \sum_{i=0}^{N} D_{ki}^{(2)} U_0(x_i)}{\partial^2 U_0(x)/\partial x^2|_{x=x_k}} \right| \tag{23}$$

versus x_k, for ρ equal to 10^4 and 1.5×10^4 and $N = 64$, 128 and 200. These results clearly demonstrate that the error is larger at the right boundary than at the left boundary. Furthermore, for $x > 0.1$ where $U(x) \approx 0$, the error increases exponentially with respect to x, reaching its largest value at the right boundary.

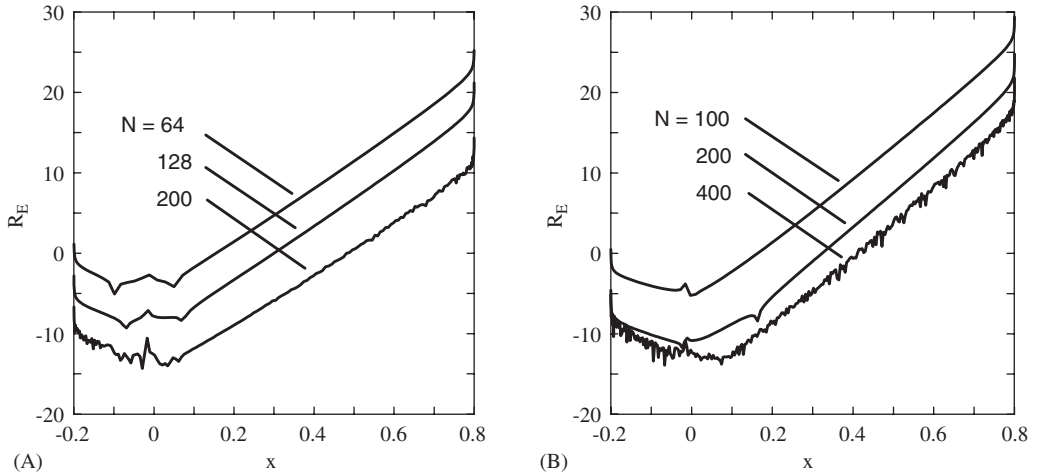

Fig. 2. The relative error versus in the application of the second derivative matrix operator to the solution at $t = 0$ for different values of N with (A) $\rho = 10,000$ and (B) $\rho = 15,000$.

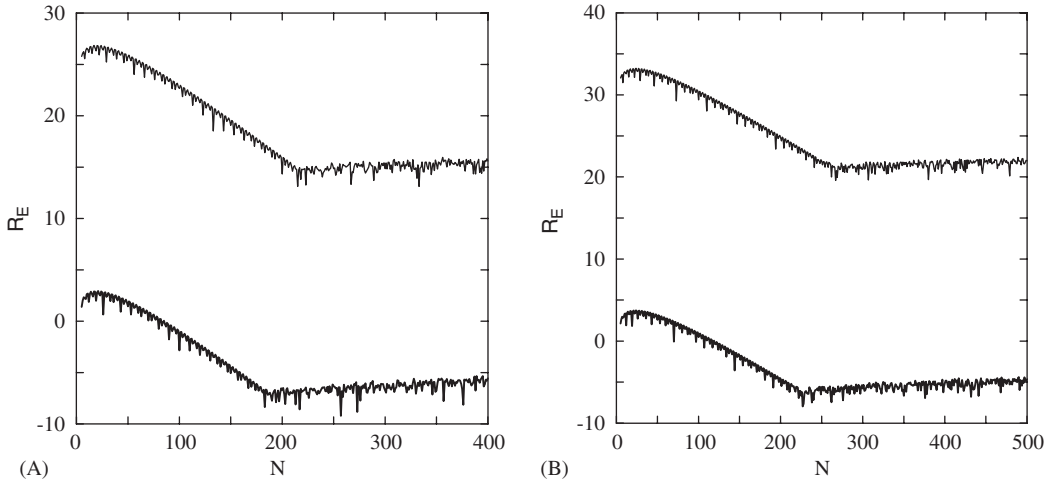

Fig. 3. The relative error R_E versus N in the application of the second derivative matrix operator to the solution at $t = 0$ at the boundaries, $x = x_R$ (upper curve) $x = x_L$ (lower curve) with ρ equal to (A) 10,000 and (B) 15,000.

In Fig. 3, the relative errors at the right and left boundaries versus N are compared. As in Fig. 2, the error is bigger at x_R than at x_L. It decreases with N until about $N = 200$ for $\rho = 10^4$ ($N = 230$ for $\rho = 1.5 \times 10^{-4}$) and then increases slowly with a further increase in N. Thus, it is clear that an increase in N decreases the error and as a consequence a stable solution can be obtained, Fig. 1(D), $N = 150$ whereas an instability occurs with a smaller $N = 64$ for Fig. 1(C). For $\rho = 10^4$, the improvement of the accuracy can be done up to $N = 200$, where for larger values of N round off error begins to become significant in the calculations. When $\rho = 1.5 \times 10^4$, $N = 250$ is not large enough to obtain a stable solution. From Fig. 3B, it is noticed that values of N greater than 250 do not provide an improvement of the accuracy due to the effects of

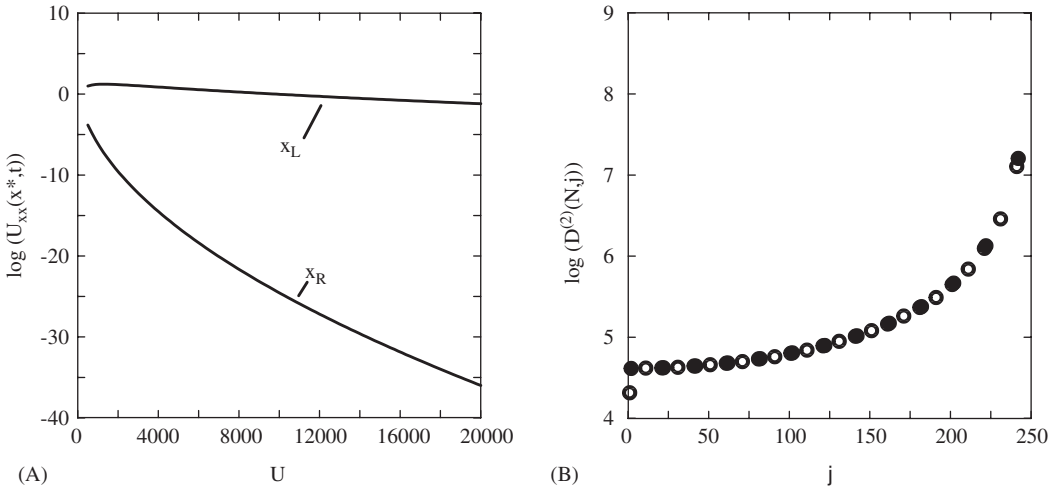

Fig. 4. (A) Variation of the logarithm of the second derivative versus ρ, at x_R and x_L for the analytic solution at $t = 0$. (B) $\log_{10}(D^2_{Nj})$ versus j. The elements alternate in sign. Negative terms (○), Positive terms (●) $N = 250$.

round-off error that have become significant. It is important to mention that round-off errors are present even for relatively small values of ρ. However, since the amplitude of the error is small throughout the time integration considered, the accumulated error does not play a crucial role, and a stable solution is obtained.

The main contribution of the round-off error, is due to (i) the alternation in sign and the magnitude of the elements of the second derivative operator $\mathbf{D}^{(2)}$, and (ii) the small values of $\partial^2 U_0(x_R)/\partial x^2$ relative to $U_0(x_L)$. $U_0(x)$ varies approximately exponentially with x for $x \approx x_R$ and $U_0(x) \approx 0$ in the region near the right boundary. Consequently, $\partial^2 U_0(x)/\partial x^2$ is very small.

The behavior of $\partial^2 U_0(x)/\partial x^2$ versus ρ at the boundary points is shown in Fig. 4A. Whereas the value of the second derivative at x_L remains almost constant, the value of $\partial^2 U_0(x_R)/\partial x^2$ is small and decreases rapidly with an increase in ρ. The numerical approximation of the second derivative at the right boundary, $\partial^2 U_0(x_R)/\partial x^2$ involves the summation of the form,

$$S_N = \sum_{k=0}^{N} D^{(2)}_{Nk} U_0(x_k), \tag{24}$$

where the subindex N refers to the Nth row and $D^{(2)}_{Ni}$ are the elements in the Nth row of the second derivative matrix operator (21). It is well-known that (i) the size of the largest element of $D^{(2)}_{Ni}$ increases as N^4, whereas the smallest increases as N^2 and (ii) the elements $D^{(2)}_{Ni}$ alternate in sign [40]. These features of the elements of $\mathbf{D}^{(2)}$ are confirmed in Fig. 4(B) for $N = 250$.

As a result, the sum (24) consists of adding alternately positive and negative terms, due to the alternation of the signs of the elements in $\mathbf{D}^{(2)}$. For $\rho = 15,000$ and $N = 250$, $\partial^2 U_0(x_R)/\partial x^2$ is of the order of 10^{-31} (Fig. 4A), whereas the terms in (24) take values from 10^{-27} to 10^4 i.e., the terms in (24) become relatively large compared to $\partial^2 U_0(x_R)/\partial x^2$.

The key point is observed in the last two elements of the sum, Eq. (24). It is the difference between two numbers of the order of 10^4, that should approximate a quantity of the order of 10^{-31}. This substraction leads to a poor approximation of the second derivative. In the same way, the approximated second derivative over the rest of the points near x_R, presents the same problem. It has to be mentioned that this problem is less severe for $\partial^2 U_0(x_L)/\partial x^2$, as $\log_{10}(\partial^2 U_0(x_L)/\partial x^2) \approx 0$.

From the previous analysis, the smallness of $\partial^2 U_0(x_R)/\partial x^2$ is the main source of round-off error at x_R. As a larger domain is considered, an increase in x_R and/or decrease in x_L, $\partial^2 U_0(x_R)/\partial x^2$ decreases, giving a larger error at x_R. Then, it is clear that the effects of round-off error are greater for a larger domain $x_R - x_L$. In order to reduce the effects of round-off error we have to consider a smaller domain. As we will see in the next section, we partition the main domain into smaller domains, contributing to a reduction in the round-off error.

From relation (12), it follows that increasing the length of the interval and fixing ρ, is equivalent to an increase of ρ and fixing the length of the interval. Then, the problem of round-off error will be present with the same magnitude whether ρ or the length of the interval are varied, according to relation (12).

The main consequence due to the round-off error problem, is the development of unwanted oscillations at some particular time step in the integration of Eq. (22). This type of oscillation is similar to the one reported in [58] for the Fourier pseudo-spectral method. The difference between the oscillations reported in [58] and the instabilities in this paper with the Chebyshev–Lobatto collocation, is the location of the oscillations. Whereas in [58] the higher amplitude oscillations are at the foot of the wave front, in this paper they are located in a neighborhood of x_R as discussed previously.

3. Chebyshev–Lobatto multidomain spectral method

In order to overcome the numerical round-off errors discussed in the previous section, we employ a multidomain approach used previously [17,18,31,38,56,57]. This involves splitting the domain $[x_L, x_R]$, into K sub-domains denoted by

$$I_\mu = [x_0^\mu, x_M^\mu],$$

where each subinterval has length L and is discretized with $M + 1$ Chebyshev points as shown in Fig. 5. The first two quadrature points of the interval $I_{\mu+1}$ coincide with the last two points of the interval I_μ.

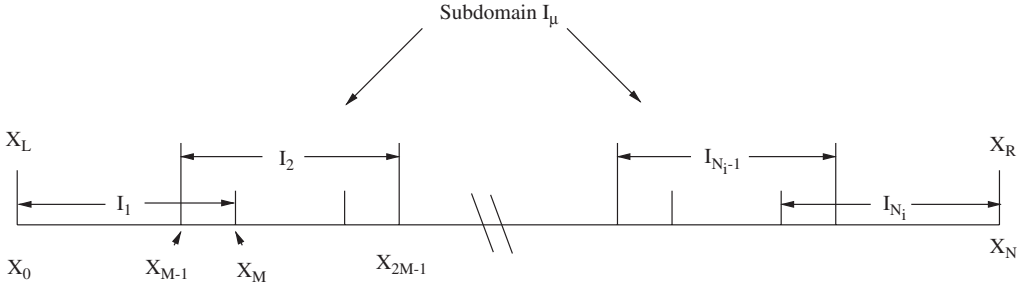

Fig. 5. Partition of the interval $[x_L, x_R]$ into N_i subdomains.

The overlap of these points of neighboring domains is possible provided that each subinterval is of the same length

$$L = \frac{x_{\mathrm{R}} - x_{\mathrm{L}}}{K + (1 - N_i)(1 - \cos(\pi/M))/2}$$

and the same number of Chebyshev collocation points is used in each interval. Thus, the new grid of points over the whole interval can be represented by

$$\{x_k\} = \{x_0^1, \ldots, x_{M-1}^1 = x_0^2, x_M^1 = x_1^2, \ldots, x_{M-2}^\mu, x_{M-1}^\mu = x_0^{\mu+1}, \ldots, x_M^K\}. \tag{25}$$

The overlap of the subdomains as described is very important for the correct construction of the derivative operators. In each sub-domain I_μ, we proceed as before and have an equation similar to Eq. (1), given by

$$\frac{\partial U^\mu}{\partial t} = \frac{\partial^2 U^\mu}{\partial x^2} + \rho U^\mu (1 - U^\mu), \quad x \in [x_0^\mu, x_M^\mu], \quad t \in [0, t_f], \tag{26}$$

where U^μ is the solution over the μth interval, and x_0^μ and x_M^μ are the left and right boundaries of the μth interval, respectively. The discretized form of Eq. (26) for each subinterval I_μ is given by

$$\frac{\mathrm{d}U_i^\mu}{\mathrm{d}t} = \frac{4}{(x_M^\mu - x_0^\mu)^2} \sum_{j=0}^{N} D_{ij}^{(2)} U_j^\mu + \rho U_i^\mu (1 - U_i^\mu), \tag{27}$$

where $U_i^\mu = U^\mu(x_i^\mu, t)$ and x_i^μ are the Chebyshev–Lobatto points over the interval I_μ. The column vector $\mathbf{U}^\mu(t)$, consists of joining the column vectors U_i^μ according to Eq. (25).

The first derivative matrix operator is then defined by,

$$D = \begin{pmatrix}
D_{0,0}^1 & D_{0,1}^1 & \cdots & D_{0,M-1}^1 & D_{0,M}^1 & & & & & \\
D_{1,0}^1 & D_{1,1}^1 & \cdots & D_{1,M-1}^1 & D_{1,M}^1 & & & & & \\
\ddots & \ddots & \ddots & \ddots & \ddots & & & & & \\
D_{M-1,0}^1 & D_{M-1,1}^1 & \cdots & D_{M-1,M-1}^1 & D_{M-1,M}^1 & & & & & \\
 & & & D_{1,0}^2 & D_{1,1}^2 & \cdots & D_{1,M-1}^2 & D_{1,M}^2 & & \\
 & & & \ddots & \ddots & \ddots & \ddots & \ddots & & \\
 & & & D_{M-1,0}^2 & D_{M-1,1}^2 & \cdots & D_{M-1,M-1}^2 & D_{M-1,M}^2 & & \\
 & & & & & & \ddots & \ddots & & \\
 & & & & & & D_{1,0}^{N_i} & D_{1,1}^{N_i} & \cdots & D_{1,M-1}^{N_i} & D_{1,M}^{N_i} \\
 & & & & & & D_{2,0}^{N_i} & D_{2,1}^{N_i} & \cdots & D_{2,M-1}^{N_i} & D_{2,M}^{N_i} \\
 & & & & & & \ddots & \ddots & \ddots & \ddots & \ddots \\
 & & & & & & D_{M,0}^{N_i} & D_{M,1}^{N_i} & \cdots & D_{M,M-1}^{N_i} & D_{M,M}^{N_i}
\end{pmatrix}$$

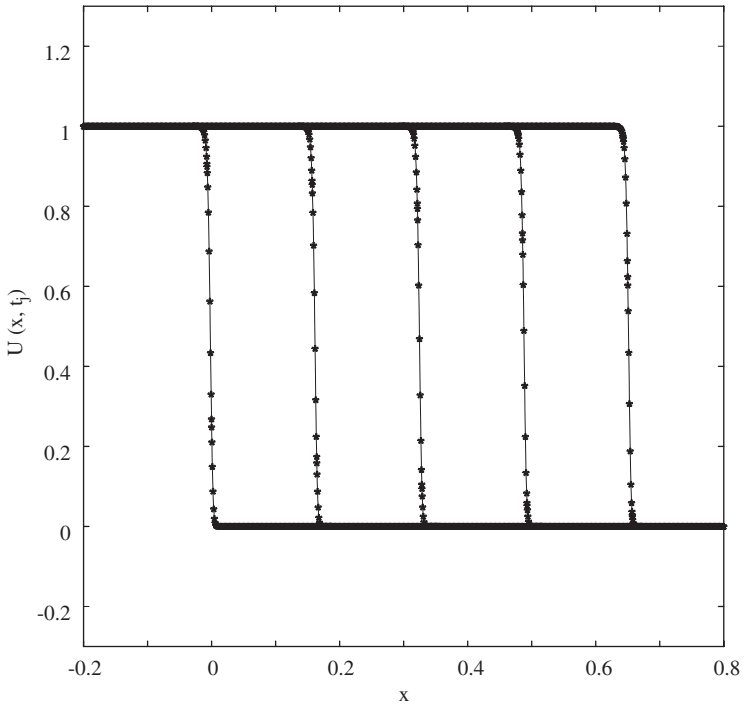

Fig. 6. Time dependent profiles $U(x,t)$ versus x for $\rho = 10^6$ with 140 subdomains and 20 points per domain; The profiles are for times $t = 8 \times 10^{-9}$, 8×10^{-5}, 1.6×10^{-4}, 2.4×10^{-4}, 3.2×10^{-4}; the total integration time is $T = 3.3 \times 10^{-4}$.

and the remaining components are zero. The size of the derivative operator is $(N+1) \times (N+1)$, with $N = M + (M-1)(K-1)$.

The multidomain approach is expected to provide more stable and accurate results. The round-off errors that occur in the application of $\mathbf{D}^{(2)}$ to the solution vector $\mathbf{U}(t)$ are smaller as the main interval has been subdivided.

We demonstrate the success of the multidomain approach in Fig. 6 where the successive profiles are shown for $\rho = 10^6$. In this calculation, 140 subdomains with 20 collocation points in each subdomain were used. The time step was $\Delta t = 8 \times 10^{-8}$ with an integration up to $T = 3.3 \times 10^{-4}$ such that $L_\infty = 3.12 \times 10^{-12}$. The agreement between the numerical and analytic solutions is excellent. The value of ρ used here is significantly larger than the value used by numerous other researchers whose works have been cited.

To further benchmark this method, we choose $\rho = 10^4$ for which we obtained accurate solutions with the single domain and $N = 150$. With the multidomain method we study the effect of varying the number of domains and the number of points in each domain. The results are summarized in Table 1. It is clear from these results that there is a considerable improvement with the multidomain method. The best results for the case in Table 1 is with 15 subdomains and 10 points per domain. The error is an order of magnitude smaller than the one domain approach with the same total number of points. In Table 2, a similar analysis is carried out for $\rho = 10^5$ with $N = 400$. The single domain calculation leads to an instability in this case. The multidomain approach provides an excellent result with 20 domains and 20 points in each domain.

Table 1
Analysis of the multidomain method for $\rho = 10^4$, $\Delta t = 10^{-8}$, total time of integration $T = 0.003$; M is the number of subintervals and N is the number of Chebyshev points per subinterval

Scheme	M (sub)	N points	L_∞ error
Chebyshev	1	150	0.332 (−2)
Multidomain	2	75	0.305 (−2)
	6	25	0.456 (−3)
	10	15	0.407 (−3)
	15	10	0.357 (−3)
	25	6	0.724 (−2)

Table 2
Analysis of the multidomain method for $\rho = 10^5$, $\Delta t = 10^{-8}$, $T = 0.001$; M is the number of subintervals and N is the number of Chebyshev points per subinterval

Scheme	M (sub)	N points	L_∞ error
Chebyshev	1	400	NAN
Multidomain	10	40	0.132 (−3)
	16	25	0.134 (−4)
	20	20	0.511 (−5)
	25	16	0.773 (−4)
	40	10	0.471 (−2)

As discussed in the previous section, $U_0(x)$ given by Eq. (5) with $t=0$, behaves as a negative exponential where $U_0(x) \approx 0$. More specifically,

$$U_0(x) \simeq \mathrm{e}^{-2\sqrt{\rho/6}x} \quad \text{for} \quad U_0(x) \approx 0. \tag{28}$$

Moreover, for values of x where $U_0(x) \approx 0$, the second derivative $\partial^2 U_0(x)/\partial x^2$ behaves like $U_0(x)$, up to a factor depending on ρ, i.e.,

$$\frac{\partial^2 U_0(x)}{\partial x^2} \simeq \frac{2\rho}{3} U_0(x) \quad \text{for} \quad U_0(x) \approx 0. \tag{29}$$

On the other hand, we know that the largest value of the sum in Eq. (24), that is used also in the multidomain approach for each subdomain, is of the order of

$$R = \log_{10}\left(\frac{4}{(x_M - x_0)^2}\right) + \log_{10}(N^2) - |\log_{10}(U_0(x_0))|, \tag{30}$$

where from Eq. (29), the smallest value to be approximated is $\partial^2 U_0(x_M)/\partial x^2 \simeq 2\rho/3 U_0(x_M)$, which is of the order of

$$E = \log_{10}\left(\frac{2\rho}{3}\right) - |\log_{10}(U_0(x_M))|. \tag{31}$$

In order to get a good approximation for E, the difference $R - E$ given by

$$R - E = \log_{10}\left(\frac{12N^2}{2\rho(x_M - x_0)^2}\right) + \log_{10}\left(\frac{U_0(x_M)}{U_0(x_0)}\right) \tag{32}$$

should be reduced. For a fixed value of ρ and N, the first term of Eq. (32) is a decreasing function of the length of the interval whereas the second is an increasing function. Then, for a fixed ρ and N there is an optimal interval length to consider in the multidomain approach.

For this last analysis, the region considered is where $U_0(x) \approx 0$. The main reason is due to the importance of having a good approximation for $U_0(x) \approx 0$, as the solution $U(x) \equiv 0$ for FE, is unstable.

4. Discrete singular convolution; Whittaker's sinc interpolation

In this section, we compare the results in Sections 2 and 3 with the results obtained with the DSC method employed in [58], to solve FE. We also provide a detailed analysis of the numerical aspects of their method. This method is based on the generic Cardinal function due to Whittaker [55] and discussed previously by others [9,16,32,45,46], and defined in terms of the sinc function,

$$C_k(x) = \frac{\sin[\pi/h(x - x_k)]}{\pi/h(x - x_k)}. \tag{33}$$

A uniform grid of $N + 1$ points $x_k = x_L + hk$, is defined for the finite interval $[x_L, x_R]$ where the grid spacing is $h = (x_R - x_L)/N$. This Cardinal function satisfies the interpolation requirement $C_k(x_j) = \delta_{jk}$, and the second derivative of $f(x)$ is approximated by

$$f_N^{(2)}(x) \approx \sum_{k=0}^{N} C_k^{(2)}(x) f(x_k). \tag{34}$$

The use of Eq. (34) on a finite interval instead of the infinite interval results in truncation errors unless the function of interest is well localized in the selected interval [9,32,45,46]. From the explicit differentiation of Eq. (33), the representation of the second derivative operator in this scheme is,

$$\tilde{D}_{jk}^{(2)} = C_k^{(2)}(x_j) = \begin{cases} -\dfrac{2(-1)^{j-k}}{(j-k)^2 h^2} & j \neq k, \\ -\dfrac{\pi^2}{3h^2} & j = k. \end{cases} \tag{35}$$

We distinguish the sinc second derivative matrix operator with a tilde overbar. This scheme is similar to the one used in [50] and by other researchers [9,16,32,45,46]. These methods employ a uniform grid based on the sinc cardinal function as the interpolation function, although they are presented from different perspectives. The time dependent solution is then determined with Eq. (22), where $A = 1$ and the derivative matrix operator given by Eq. (35). Although Wei [51,52] presents his methodology in the language of wavelets and signal analysis, it is useful to recognize that it is simply an alternate interpolation scheme analogous to other interpolations schemes such as Lagrange [6,32,42] as well as the interpolation defined in terms of orthogonal polynomials in Section 2.2.

We present an analysis of the numerical aspects of the DSC method with concern to the round-off errors associated with the application of the second derivative matrix operator, $\tilde{\mathbf{D}}^{(2)}$, to $U_0(x)$ and to

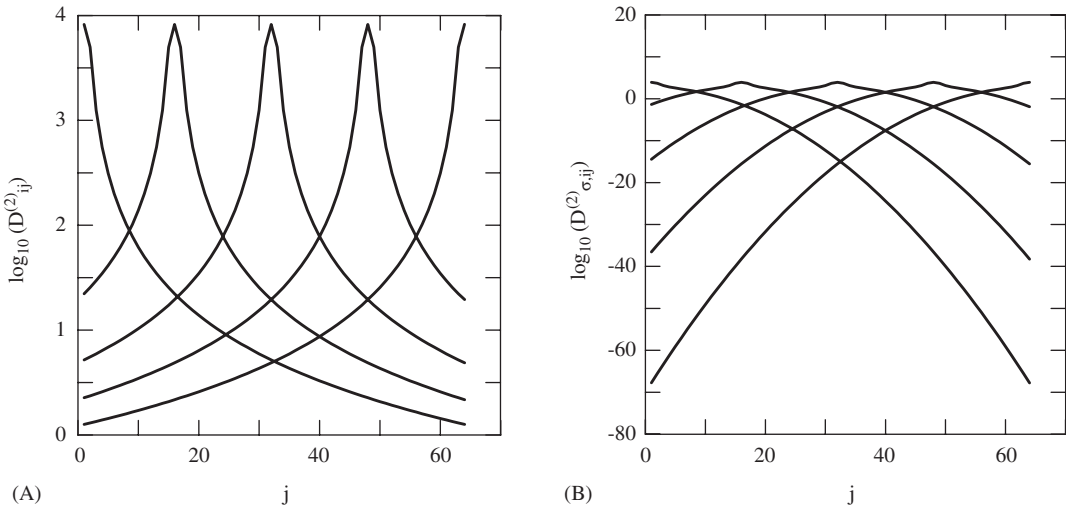

Fig. 7. Logarithmic value of the ith row of (A) $\mathbf{D}^{(2)}$ (B) $\mathbf{D}^{(2)}_{\sigma}$, for $i = 1$, 16, 32, 48 and 64. The largest value occurs for $j = i$.

FE analogous to the analysis for $\mathbf{D}^{(2)}$ in Section 2.3. Zhao and Wei [58] report excellent results for the solution of FE. It is useful to consider a detailed analysis of the second derivative matrix operator that they used analogous to the study in Section 2.3 of the Chebyshev–Lobatto spectral method.

As the sinc function decays slowly as $1/x$, Zhao and Wei [58] multiplied the sinc function in Eq. (33) with a Gaussian window function of the form $R_\sigma(x) = \exp(-x^2/2\sigma^2)$ such that

$$C_{\sigma,k} = \frac{\sin[\pi/h(x - x_k)]}{\pi/h(x - x_k)} \exp\left(-\frac{(x - x_k)^2}{2\sigma^2}\right). \tag{36}$$

Thus, the second derivative matrix operator matrix $\tilde{\mathbf{D}}^{(2)}$ is thus changed to $\mathbf{D}^{(2)}_{\sigma}$ with elements,

$$D^{(2)}_{\sigma,jk} = \begin{cases} \dfrac{2(-1)^{j-k+1}}{h^2}\left(2\gamma + \dfrac{1}{(j-k)^2}\right)\exp(-\gamma(j-k)^2) & j \neq k, \\ -\dfrac{1}{3}\left(\dfrac{3}{\sigma^2} + \dfrac{\pi^2}{2\gamma\sigma^2}\right) & j = k, \end{cases} \tag{37}$$

where $\gamma = h^2/2\sigma^2$. As $R_\sigma(x)$ is a Gaussian and $R_\sigma(0) = 1$, only the off-diagonal elements of $\tilde{\mathbf{D}}^{(2)}$ are modified. Zhao and Wei [58] chose the optimum value $\sigma = 3.5h$. Chen and Shizgal [15,14] employed a similar weighted interpolation scheme for the solution of Sturm–Liouville problems and the Poisson equation. This was originally proposed by Weideman [53].

We show the matrix elements of the kth row of $\log_{10}(\tilde{D}^{(2)}_{jk})$ and $\log_{10}(D^{(2)}_{\sigma,jk})$ in Figs. 7(A) and (B), respectively, versus j for fixed $k = 1$, 16, 32, 48 and 64, and $N = 64$. From the results in Fig. 7(A), we see that the matrix elements of $\tilde{\mathbf{D}}^{(2)}$ are of the order 10^4 along the diagonal and decay quickly away from the diagonal. This should be compared with the matrix elements of $\mathbf{D}^{(2)}_{\sigma}$ whose elements range from 10^4 on the diagonal to as small as about 10^{-65} for the extreme off-diagonal elements. The addition of the Gaussian window function has resulted in a rapid decrease of the derivative matrix operator away from the diagonal as expected, and thus the derivative matrix is banded about the diagonal.

We consider an additional modification of the differentiation algorithm, Eq. (34), such that

$$f_N^{(2)}(x_j) \approx \sum_{k=k_{\min}}^{k_{\max}} D_{\sigma,jk}^{(2)} f(x_k), \tag{38}$$

where

$$k_{\min} = \begin{cases} 0 & j < W, \\ j - W & j \geqslant W, \end{cases} \quad \text{and} \quad k_{\max} = \begin{cases} W + j & j \leqslant N - W, \\ N & j > N - W \end{cases} \tag{39}$$

and W is the number of elements on either side of the diagonal that are retained with $2W + 1 < N$. The elements of $\mathbf{D}_\sigma^{(2)}$ decay exponentially as we move away from the diagonal due to the introduction of the Gaussian window function in Eq. (36). From Fig. 7B we see that the terms neglected vary from about 10^{-16} to 10^{-67}. This should not influence the final results as these elements of $\mathbf{D}_\sigma^{(2)}$ are small. This procedure reduces the bandwidth (RB) from N to $2W + 1$ and the derivative algorithm is now more local than global. In the next section, we report an analysis of the two second derivative matrix operators, $\tilde{\mathbf{D}}^{(2)}$, $\mathbf{D}_\sigma^{(2)}$ given by (35) and (37), respectively, with and without RB. While the polynomial interpolation, Eq. (19), and the associated differentiation algorithm, Eq. (21), can give excellent results on a finite interval, the interpolation based on the Sinc functions, Eq. (34), and the differentiation algorithm, Eq. (38), involve truncation errors especially at the boundaries of the finite interval $[x_L, x_R]$. With this in mind, we consider an alternative interpretation of Eq. (38) whereby the differentiation algorithm is always centred on the point x_k with W points to the left and W points to the right of the point of interest. Thus we define a second derivative matrix operator $\overline{\mathbf{D}}_\sigma^{(2)}$ which is of dimension $(N + 2W + 1) \times (N + 1)$ and operates on solution vectors of FE of dimension $(N + 2W + 1)$ of the form

$$(1, 1, \ldots, 1, U(x_0) = U(x_L) = 1, U(x_1), \ldots, U(x_N) = U(x_R) = 0, 0 \ldots 0, 0)$$

with the first W components set equal to unity and the last W components set equal to zero consistent with the boundary conditions. The $(N + 1)$ components $U(x_i)$ are computed from the solution of FE within the computational domain $[x_L, x_R]$.

4.1. Analysis of the round-off error for $\tilde{\mathbf{D}}^{(2)}$, $\mathbf{D}_\sigma^{(2)}$ and $\overline{\mathbf{D}}_\sigma^{(2)}$

We consider a solution of FE with the same values used in Section 2.3, that is, $x_L = -0.2$, $x_R = 0.8$, $\rho = 10^4$ and $N = 64$. In Fig. 8, we show the computed profile after the first time step for $\tilde{\mathbf{D}}^{(2)}$ without RB in Fig. 8(A) and with RB in Fig. 8(B). In both cases, small amplitude oscillations develop at the foot of the wave front. These oscillations are responsible for the unstable numerical solutions that are obtained. On the other hand, when the window function R_σ is considered, i.e. the second derivative operator matrix is given by $\mathbf{D}_\sigma^{(2)}$, there are no oscillations. As a result, a stable solution is obtained.

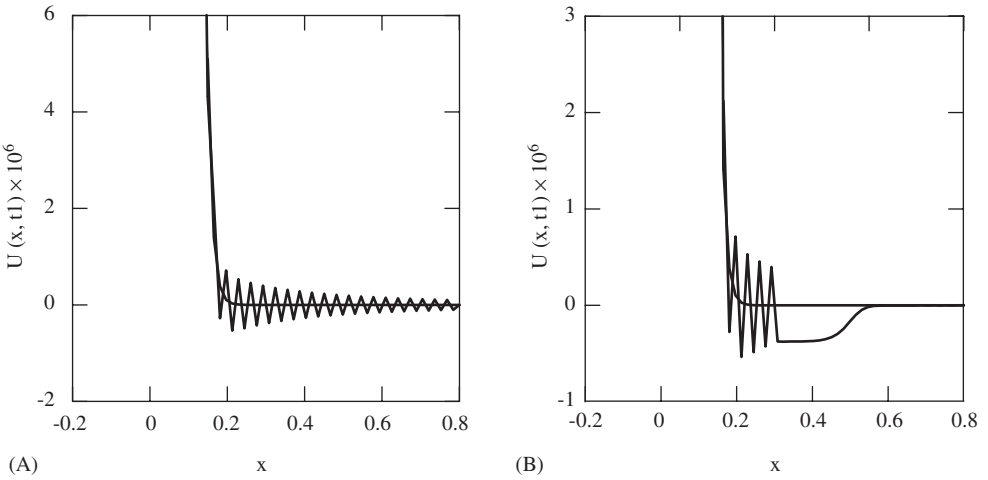

Fig. 8. Oscillations of $U(x,t)$ after the first time step. $\mathbf{D}^{(2)}$ is given by (35). (A) Without reduced bandwidth (RB), (B) With RB. $\rho = 10^4$, $N = 64$.

To understand the origin of the oscillations when the operator $\tilde{\mathbf{D}}^{(2)}$ with and without RB is considered, we study the details in the sum involved in the calculation of the second derivative of $U_0(x)$, given by

$$S_j = \sum_{k=0}^{N} \mathscr{L}_{jk} U_0(x_k), \tag{40}$$

where the matrix operator $\mathscr{L}$ can be $\tilde{\mathbf{D}}^{(2)}$ or $\mathbf{D}_\sigma^{(2)}$ with or without RB. For the present analysis, two test points $x = 0.3$ and $x = 0.8$, which correspond to $j = N/2$ and $j = N$, respectively, were considered to approximate the second derivative. The elements in the sum in Eq. (40) alternate in sign along a row, as shown in Eqs. (35) and (37). The calculation of the second derivative for $j = N/2$ and $j = N$, is subject to round-off errors analogous to the discussion in Section 2.3. The values $\partial^2 U_0(x_{N/2})/\partial x^2 = 2.93 \times 10^{-7}$ and $\partial^2 U_0(x_N)/\partial x^2 = 2.85 \times 10^{-25}$ ($N = 64$, $N/2 = 32$) are approximated by a difference of two numbers whose order will depend on the second derivative operator matrix $\mathscr{L}$.

A summary of the order of magnitude of the elements, whose difference will approximate $\partial^2 U_0(x_{32})/\partial x^2$ and $\partial^2 U_0(x_{64})/\partial x^2$ for different second derivative operators $\mathscr{L}$, is presented in Table 3. For the case of $\tilde{\mathbf{D}}^{(2)}$ without RB, both $\partial^2 U_0(x_{32})/\partial x^2 = 2.93 \times 10^{-7}$ and $\partial^2 U_0(x_{64})/\partial x^2 = 2.85 \times 10^{-25}$ are approximated by the difference of two numbers of the order of 10^1. This round-off error problem is similar to the problems encountered with Chebyshev Lobatto collocation discussed previously. The result of such round-off error is shown in Fig. 8(A).

Similar instabilities are obtained when $\tilde{\mathbf{D}}^{(2)}$ with RB is considered. However, as seen in Fig. 8(B), there is a notable improvement after the first time step integration for $x = x_{64}$. This improvement is a consequence of the approximation of $\partial^2 U_0(x_{64})/\partial x^2$, that is calculated as a difference of two numbers of the order of 10^{-9} (Table 3).

On the other hand, when $\mathbf{D}_\sigma^{(2)}$ given by (37) with and without RB is considered, the solution is free of oscillations and as a consequence, a stable solution is obtained. The results in Table 3, show the improvement of the approximation of the second derivative at $x = x_{32}$ and $x = x_{64}$.

Table 3
Maximum value of the elements in the sum, Eq. (40), with $\mathscr{L}$ equal to $\mathbf{D}^{(2)}$ and $\mathbf{D}_\sigma^{(2)}$

Operator	$\frac{\partial^2 U_0(x_{32})}{\partial x^2} = 2.93 \times 10^{-7}$	$\frac{\partial^2 U_0(x_{64})}{\partial x^2} = 2.85 \times 10^{-25}$
$\mathscr{L}$	$\mathrm{Max}_k \quad \mathscr{L}_{32k} U_0(x_k)$	$\mathrm{Max}_k \quad \mathscr{L}_{64k} U_0(x_k)$
$\mathbf{D}^{(2)}$ (No RB)	10^1	10^1
$\mathbf{D}^{(2)}$ (RB)	10^1	10^{-9}
$\mathbf{D}_\sigma^{(2)}$ (No RB)	10^{-4}	10^{-21}
$\mathbf{D}_\sigma^{(2)}$ (RB)	10^{-4}	10^{-21}

When reduced bandwidth (RB) is considered, the index in the sum, Eq. (40), runs from $-W$ to W, $W = 32$.

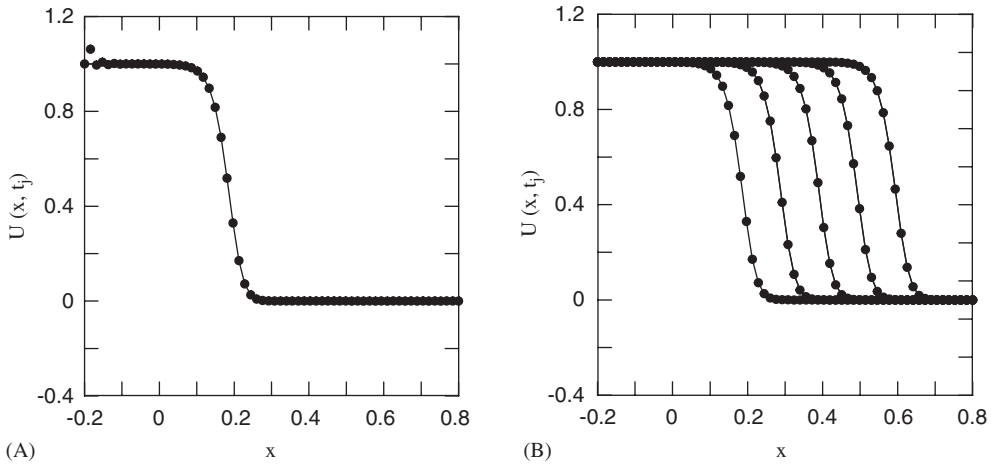

Fig. 9. (A) Instability of $U(x, t)$ at $x = x_L$, $\rho = 10^4$, $\Delta t = 1 \times 10^{-7}$. The $(N+1) \times (N+1)$ second derivative operator considered is $\mathbf{D}_\sigma^{(2)}$ given by the algorithm, Eqs. (38) and (39); $N = 64$; total integration time $T = 0.004$. (B) Time dependent profiles versus x for $\rho = 10^4$ and times $t = 0.001$, 0.0015, 0.002, 0.0025 and 0.003 with the $(N + 2W + 1) \times (N + 1)$ second derivative operator $\overline{\mathbf{D}}_\sigma^{(2)}$; $N = 64$, $W = 32$.

It is important to mention that the approximation of $\partial^2 U_0(x_{64})/\partial x^2 = 2.85 \times 10^{-25}$, with $\mathbf{D}_\sigma^{(2)}$, is numerically inaccurate even though the elements of the sum Eq. (40) range from 10^{-26} to 10^{-21}. The inaccurate approximation is due in part to the use of the window function R_σ, that modifies the structure of the elements of $\tilde{\mathbf{D}}^{(2)}$. Since the error in the calculation of $\partial^2 U_0(x_{64})/\partial x^2$ is at most of the order of 10^{-21}, the error generated is small for the time integration considered. This, leads to an excellent solution for FE with large values of ρ.

In Fig. 9(A) we show the solution to FE with $\mathbf{D}_\sigma^{(2)}$. We find a small growing instability near $x = x_L$ after several time steps and which after some time ceases to grow. We find that the amplitude of this instability increases with N.

The origin of the instability near $x = x_L$ in Fig. 9(A), can be understood in terms of the second derivative operator $\mathbf{D}_\sigma^{(2)}$ applied to $U_0(x)$. From Eq. (38), $S_0 \approx \mathrm{O}(10^4)$ is the approximation of $\partial^2 U_0(x_0)/\partial x^2 = \mathrm{O}(10^0)$. This poor approximation is due to the truncation of the physical domain to $[x_L, x_R]$. The effect of

the truncation on the approximation of $\partial^2 U_0(x_k)/\partial x^2$ depends directly on the combination of the values of $U_0(x_k)$ and $D^{(2)}_{\sigma,0k}$ in Eq. (38). For $x = x_L$, the largest value of both $U_0(x_k)$ and $D^{(2)}_{\sigma,0k}$ is for $k = 0$, and thus the main contribution of the sum, Eq. (38), is from the first element with magnitude 10^4. Therefore, if the vector U_n denotes the numerical solution at the nth time step, we find that $U_n(x_2) \to \eta \neq 1$ as $n \to \infty$, as shown in Fig. 9(A). In this case η satisfies the relation

$$\lim_{n\to\infty} D^{(2)}_{\sigma} U_n|_{x=x_2} = \rho\eta(1-\eta). \tag{41}$$

From Eq. (41), it is shown that for any time $t = t_n$ the poor approximation of $\partial^2 U_0(x_0)/\partial x^2$ at $x = x_1$ is always present and $S_0 \approx \mathrm{O}(10^4)$ for $t = t_n$.

However, when $x = x_R$, the truncation of the domain does not have the same effect as the one shown in Fig. 9 for $x = x_L$. The quantity to be approximated is of the order of 10^{-25} whereas the largest element of Eq. (38) for $x = x_R$ is also of the order of 10^{-25}.

However, the instability that occurs near $x = x_L$, does not destabilize the rest of the solution. This is due to the distribution of the elements of $\mathbf{D}^{(2)}_{\sigma}$ as shown in Fig. 7(B), and the magnitude of elements of $U_0(x)$. In order to approximate $\partial^2 U_0(x)/\partial x^2$ near $x = x_R$, the values of $U_0(x)$ near $x = x_L$ do not play any role in the calculation, even if RB is not considered. This is an important difference between Chebychev–Lobatto collocation and the weighted DSC (Eq. (37)) differentiation matrices, applied to FE. Whereas in Chebychev–Lobatto collocation, the second derivative at some point $x = x_k$ has a strong dependence on all the Chebychev–Lobatto points, that is, is global, the DSC with the window function becomes a more local method as only a small number of points, play a major role in the calculations. It is important to mention that for a fixed value of ρ, x_L and x_R, it is not possible to eliminate the instability at $x = x_L$ in Fig. 9(A). One possible alternative to get a good solution on x_L and x_R, is to increase the physical domain, keeping only the interval in x where the solution has a good precision. However, this alternative will break the structure given by ρ, x_L and x_R in relation (12), giving as a result a different numerical problem.

However, when the solution vector is "padded" with W points to the left of x_L and W points to the right of x_R such that

$$U(x_k) = \begin{cases} 1 & \text{if } -W \leqslant k \leqslant -1, \\ 0 & \text{if } N+1 \leqslant k \leqslant N+W \end{cases} \tag{42}$$

and $\overline{\mathbf{D}}^{(2)}_{\sigma}$ of dimension $(N+2W+1)\times(N+1)$ is used, we obtain the result shown in Fig. 9(B) without the instability at $x = x_L$ shown in Fig. 9(A). In this calculation with $\rho = 10^4$ and $x \in [-0.2, 0.8]$, we verified that both $\partial^2 U_0(x)/\partial x^2|_{x=x_1}$ and its numerical approximation S_0 given by Eq. (40) are of order one O(1). Again the approximation of $\partial^2 U_0(x)/\partial x^2|_{x=x_1}$ is numerically inaccurate, due to the use of the window function R_σ and because $U(x)$ lies outside the space of bandlimited functions as described in [46]. However, the numerical solution that is obtained is accurate as now $\eta = 1$ in Eq. (41). Therefore, we obtain

$$\lim_{n\to\infty} D^{(2)}_{\sigma} U_n|_{x=x_1} = \rho\eta(1-\eta) = 0 \tag{43}$$

giving as a result what is shown in Fig. 9(B). Table 4 shows a comparison between the results with the sinc method with $\overline{D}^{(2)}_{\sigma}$ and the multidomain method presented in Section 3. The multidomain approach provides a more accurate result for the largest value of ρ.

Table 4
Comparison between multidomain method and the Sinc approach with $\overline{\mathbf{D}}_{\sigma}^{(2)}$ (W = 32) for different values of ρ

Scheme	ρ	M (sub)	N points	Δt	T	L_∞ error
Sinc	10^4	1	75	1×10^{-7}	0.0032	4.976 (−4)
	10^5	1	400	1×10^{-8}	0.001	1.395 (−10)
	10^6	1	2800	1×10^{-8}	0.00033	4.966 (−8)
Multidomain	10^4	3	25	1×10^{-7}	0.0032	4.839 (−3)
	10^5	20	20	1×10^{-8}	0.001	5.115 (−6)
	10^6	140	20	8×10^{-8}	0.00033	3.125 (−12)

T is the total time of integration, M is the number of subintervals and N is the number of Chebyshev points per subinterval.

5. Summary

The objective of the present paper was to develop an accurate and efficient pseudospectral solution of the FE, a prototypical reaction–diffusion equation. The collocation method used the Chebyshev–Gauss–Lobatto quadrature points. The solutions of FE are characterized by propagating fronts that can be steep depending on the value of the reaction rate coefficient, ρ. We compared results for a single domain as well as for a subdivision of the main domain into subintervals. On a single domain the integration of the FE lead to instabilities at some time step. These instabilities were a consequence of the numerical round-off errors arising from the numerical form of the discrete second-order derivative matrix operator. We have demonstrated the importance of constructing the differential matrix operator accurately. From a detailed numerical analysis, we have also identified the nature of the round-off errors that occur in the use of the differential matrix operator in the numerical solution of FE. This complements the work in [5]. The exponentially small values of the solution, $U(x, t)$, combined with the size of the elements in $\mathbf{D}^{(2)}$ which oscillate in sign along a row, was the main source of round-off error, when a single domain was used.

In order to reduce the effects of round-off error for the Chebyshev collocation, the main domain was subdivided into smaller subintervals as proposed in [31,56,57]. The multidomain method provided stable and accurate solutions of FE for values of ρ as large as 10^6. We also compared the present numerical treatment with the DSC approach of Zhao and Wei [58] who employed an interpolation based on the sinc function. They added a window function R_σ to the sinc interpolation function and also limited the number of terms in the differentiation algorithm to a small number about the diagonal elements of the derivative matrix operator. We refer to this procedure as reduced bandwidth RB. We also studied the occurrence of numerical round-off with their method. We found that for fixed values of ρ, x_L and x_R, the results with the multidomain method did not present any problem at the left boundary at $x = x_L$ as did the DSC method. The instability at the left boundary shown in Fig. 9(A) obtained with DSC, is attributed to the truncation of the spatial domain as discussed in Section 4.1.

Another important result of this paper is the demonstration of the equivalence of the numerical problems defined by Eqs. (6)–(8) and Eqs. (10), (11). However, for Eqs. (6)–(8), the parameter ρ plays an important role and for large ρ we have the SSW situation, whereas for Eqs. (10), (11) the main parameter is the length of the numerical domain. The results in the present paper for Fisher's equation, a prototypical

reaction–diffusion equation, will play an important role in the application of pseudospectral methods to more complex physical systems such as the Fitzhugh–Nagumo equation [20,37].

Acknowledgements

This research is supported in part by a grant to BDS from the Natural Science and Engineering Research Council of Canada, and a graduate scholarship to DO from the Mexican Consejo Nacional de Ciencia y Tecnología (CONACYT). We are grateful to Dr. Jae-Hun Jung for several useful discussions.

References

[1] M.J. Ablowitz, A. Zepetella, Explicit solutions of Fisher's equation for a special wave speed, Bull. Math. Biol. 41 (1979) 835–840.
[2] K. Al-Khaled, Numerical study of Fisher's reaction–diffusion equation by the sinc collocation method, J. Comput. Appl. Math. 137 (2001) 245–255.
[3] R. Baltensperger, Improving the accuracy of the matrix differentiation method for arbitrary collocation points, Appl. Numer. Math. 33 (2000) 143–149.
[4] R. Baltensperger, J.P. Berrut, The errors in calculating the pseudospectral differentiation matrices for Chebyshev–Gauss–Lobatto points, Comput. Math. Appl. 37 (1999) 41–48.
[5] R. Baltensperger, M.R. Trummer, Spectral differencing with a twist, SIAM J. Sci. Comput. 24 (2003) 1465–1487.
[6] D. Baye, M. Hesse, M. Vincke, The unexplained accuracy of Lagrange mesh-method, Phys. Rev. E 65 (2002) 026701 1–8.
[7] G. Beckett, J.A. Mackenzie, A. Ramage, D.M. Sloan, On the numerical solution of one-dimensional PDEs using adaptive methods based on equidistribution, J. Comput. Phys. 167 (2001) 292–372.
[8] G. Beckett, J.A. Mackenzie, A. Ramage, D.M. Sloan, Computational solution of two-dimensional unsteady PDEs using moving mesh methods, J. Comput. Phys. 182 (2002) 478–495.
[9] J.P. Boyd, Chebyshev and Fourier Spectral Methods, Dover, New York, 2000.
[10] P.K. Brazhnik, J.J. Tyson, On travelling wave solutions of Fisher's equation in two spatial dimensions, SIAM J. Appl. Math. 60 (1999) 371–391.
[11] J. Canosa, On a nonlinear diffusion equation describing population growth, IBM J. Res. Develop. 17 (1973) 307–313.
[12] C. Canuto, M.Y. Hussaini, A. Quarteroni, T.A. Zang, Spectral Methods in Fluid Dynamics, Springer Series in Computational Physics, Springer, New York, 1988.
[13] G.F. Carey, Y. Shen, Least-squares finite element approximation of Fisher's reaction–diffusion equation, Numer. Methods Partial Differential Equations 11 (1995) 175–186.
[14] H. Chen, B.D. Shizgal, A spectral solution of the Sturm–Liouville equation; comparison of classical and nonclassical polynomials, J. Comput. Phys. 136 (2001) 17–35.
[15] H. Chen, Y. Su, B.D. Shizgal, A direct spectral collocation Poisson solver in polar and cylindrical coordinates, J. Comput. Phys. 160 (2000) 453–469.
[16] D.T. Colbert, W.H. Miller, A novel discrete variable representation for quantum mechanical reactive scattering via the S-matrix Kohn method, J. Chem. Phys. 196 (1992) 1982–1991.
[17] P.J. Diamessis, J.A. Domaradzki, J.S. Hesthaven, A spectral multidomain penalty method model for the simulation of high Reynolds number localized incompressible stratified turbulence, J. Comput. Phys. 202 (2005) 298–322.
[18] W.S. Don, D. Gottlieb, J.-H. Jung, A multidomain spectral method for supersonic reactive flows, J. Comput. Phys. 192 (2003) 325–354.
[19] R.A. Fisher, The wave of advance of advantageous genes, Ann. Eugenics 7 (1937) 355–369.
[20] R. Fitzhugh, Impulses and physiological states in theoretical models of nerve membrane, Biophys. J. 1 (1961) 445–466.
[21] J. Gazdag, J. Canosa, Numerical solution of Fisher's equation, J. Appl. Probab. 11 (1974) 445–457.
[22] D. Gottlieb, J.S. Hesthaven, Spectral methods for hyperbolic problems, J. Comput. Appl. Math. 128 (2001) 83–131.
[23] S.A. Gourley, Travelling front solutions of a nonlocal Fisher equation, J. Math. Biol. 41 (2000) 272–284.

[24] P. Hagan, Travelling wave and multiple travelling wave solutions of parabolic equations, SIAM J. Math. Anal. 13 (1982) 717–738.
[25] T. Hagstrom, H.B. Keller, The numerical calculation of travelling wave solutions of nonlinear parabolic equations, SIAM J. Sci. Statist. Comput. 7 (1986) 978–988.
[26] W. Huang, Y. Ren, R.D. Russell, Moving mesh partial differential equations (MMPDEs) based on the equidistribution principle, SIAM J. Numer. Anal. 31 (1994) 709–730.
[27] W. Huang, R.D. Russell, A moving collocation method for solving time dependent partial differential equations, Appl. Numer. Math 20 (1996) 101–116.
[28] A. Kolmogorov, I. Petrovsky, N. Piscounov, Étude de l'équation de la diffusion avec croisance de la quantité de matière et son application á un problème biologique, Bull. Univ. Etat. Moscu A 1 (1937) 1–25.
[29] D.A. Larson, Transient bounds and time-asymptotic behavior of solutions to nonlinear equations of Fisher type, SIAM J. Appl. Math. 34 (1978) 93–103.
[30] S. Li, L. Petzold, Y. Ren, Stability of moving mesh systems of partial differential equations, SIAM J. Sci. Comput. 20 (1998) 719–738.
[31] G. Mansell, W. Merryfield, B. Shizgal, U. Weinert, A comparison of differential quadrature methods for the solution of partial differential equations, Comp. Methods Appl. Mech. Engrg. 104 (1993) 295–316.
[32] E.H.W. Meijering, W.J. Niessen, Viergeveer, The Sinc approximating kernels of classical polynomial interpolation, IEEE Conf. Image Proc. 3 (1999) 652–656.
[33] R.E. Mickens, A best finite-difference scheme for Fisher's equation, Numer. Meth. Part. D. E. 10 (1994) 581–585.
[34] R.E. Mickens, Relation between the time and space step-sizes in nonstandard finite difference schemes for the Fisher equation, Numer. Meth. Part. D. E. 13 (1997) 51–55.
[35] L.S. Mulholland, Y. Qiu, D.M. Sloan, Solution of evolutionary partial differential equations using adaptive finite differences with pseudospectral post-processing, J. Comput. Appl. Math. 131 (1997) 280–298.
[36] J.D. Murray, Mathematical Biology I: An Introduction, third ed., Springer, New York, 2002.
[37] J. Nagumo, S. Arimoto, S. Yoshizawa, An active pulse transmission line simulating nerve axon, Proc. IRE 50 (1962) 2061–2070.
[38] S.A. Nielsen, J.S. Hesthaven, A multi-domain Chebyshev collocation method for predicting ultrasonic field parameters in complex material geometries, Ultrasonics 40 (2002) 177–180.
[39] N. Parekh, S. Puri, A new numerical scheme for the Fisher equation, J. Phys. A 23 (1990) L1085–L1091.
[40] R. Peyret, Spectral Methods for Incompressible Viscous Flow, Springer, New York, 2002.
[41] Y. Qiu, D.M. Sloan, Numerical solution of Fisher's equation using a moving mesh method, J. Comput. Phys. 146 (1998) 726–746.
[42] R.E. Robson, K.F. Ness, G.E. Sneddon, L.A. Viehland, Comment on the discrete ordinate method in the kinetic-theory of gases, J. Comput. Phys. 92 (1991) 213–229.
[43] Rizwan-Uddin, Comparison of the nodal integral method and non standard finite-difference schemes for the Fisher equation, SIAM. J. Sci. Comput. 22 (2001) 1926–1942.
[44] J. Roessler, H. Hüssner, Numerical solution of the $1+2$ dimensional Fisher's equation by finite elements and the Galerkin method, Math. Comput. Modelling 25 (1997) 57–67.
[45] C. Schwartz, High accuracy approximation techniques for analytic functions, J. Math. Phys. 26 (1985) 411–415.
[46] C.E. Shannon, Communication in the presence of noise (Classic paper), Proc. of the IEEE 86 (1998) 447–457.
[47] F. Stenger, Numerical methods based on sinc and analytic functions, Springer Ser. Comput. Math. 20 (1993) 91–96.
[48] S. Tang, R.O. Weber, Numerical study of Fisher's equation by a Petrov Galerkin finite element method, J. Austral. Math. Soc. Sci. B 33 (1991) 27–38.
[49] E.H. Twizell, Y. Wang, W.G. Price, Chaos free numerical solutions of reaction–diffusion equations, Proc. Roy. Soc. London Sci. A. 430 (1990) 541–576.
[50] G.W. Wei, Solving quantum eigenvalue problems by discrete singular convolution, J. Phys. B 33 (2000) 343–352.
[51] G.W. Wei, A unified approach for the solution of the Fokker–Planck equation, J. Phys. A 33 (2000) 4935–4953.
[52] G.W. Wei, A new algorithm for solving some mechanical problems, Comput. Methods Appl. Mech. Engrg. 190 (2001) 2017–2030.
[53] J.A.C. Weideman, Spectral methods based on nonclassical orthogonal polynomials, Internat. Ser. Numer. Math. 131 (1999) 238–251.
[54] J.A.C. Weideman, S.C. Reddy, A MATLAB matrix differentiation suite, ACM Trans. Math. Software 26 (2000) 465–519.

[55] E.T. Whittaker, On the functions which are represented by the expansions of the interpolation theory, Proc. Roy. Soc. Edinburgh 35 (1915) 181–194.
[56] H. Yang, B. Shizgal, Chebyshev pseudospectral multidomain technique for viscous flow calculation, Comput. Methods Appl. Mech. Engrg. 118 (1994) 47–61.
[57] H. Yang, B. Seymour, B. Shizgal, A Chebyshev pseudospectral multidomain method for steady flow past a cylinder, up to Re = 150, Comput. Fluids 23 (1994) 829–851.
[58] S. Zhao, G.W. Wei, Comparison of the discrete singular convolution and three other numerical schemes for solving Fisher's equation, SIAM J. Sci. Comput. 25 (2003) 127–147.
[59] X. Zou, Delay induced traveling wave fronts in reaction–diffusion equations of KPP-Fisher type, J. Comput. Appl. Math. 146 (2002) 309–321.